Synthesis, Crystal Structures, and Magnetic Properties of Double Perovskites Containing 5d Transition Metals

Senior Thesis

Presented in partial fulfillment of the requirements for graduation with research distinction in Chemistry in the undergraduate colleges of The Ohio State University

by

Nathalie Milbrandt

The Ohio State University
May 2018

Project Advisor: Dr. Patrick Woodward, Department of Chemistry and Biochemistry

TABLE OF CONTENTS

Abstract

Transition metal oxides containing 5*d* ions have exhibited many exotic magnetic properties, the underlying mechanisms of which have not yet been fully understood. Many of the unique characteristics of 5*d* transition metal oxides are thought to be dependent on the strong spin-orbit coupling and the extended d-orbitals. Double perovskites provide a great platform to study the magnetic interactions among 5*d* transition metal ions because they are amenable to various types of elemental substitutions. For $5d^1$ and $5d^2$ electron configurations, magnetic properties such as ferromagnetism, antiferromagnetism, and spin glass have been observed.[1] Octahedrally coordinated transition metal ions with a $5d^4$ configuration should possess a nonmagnetic J=0 ground state, due to the effects of strong spin-orbit coupling. However, recent studies have shown that non-trivial magnetic moments exist in some compounds.[2,3] By synthesizing new perovskites containing 5d transition metals, the exotic magnetic properties can be explored.

Solid-state synthesis has been performed of targeted stoichiometries of Sr_2ZnReO_6, which is in a d^1 configuration, and Ba_2MIrO_6 (M= Lu, Fe), $Ba_3Fe_2IrO_9$, and SrLaM'IrO_6 (M'= Zn, Mg, and Ni), which contain ions with a $5d^4$ configuration. The crystal structures of the products have been studied using X-ray powder diffraction. Sr_2ZnReO_6 crystallizes in a tetragonal double perovskite structure, Ba_2LuIrO_6 crystallizes in a cubic double perovskite structure, $Ba_2Fe_{1.257}Ir_{0.743}O_6$ and $Ba_2Fe_{1.05}Ir_{0.95}O_6$ crystallize in a trigonal structure, and all the other iridates crystallize in a monoclinic double perovskite structure. Magnetic data shows that Ba_2LuIrO_6, SrLaZnIrO_6, and SrLaMgIrO_6 are paramagnetic, SrLaNiIrO_6 , SrLaNiNbO_6, and SrLaNiTaO_6 are antiferromagnetic, and Sr_2ZnReO_6 is ferromagnetic. This study is expected to expand our knowledge of the interesting magnetic phenomena presented by 5*d* transition metal oxides in different crystal structures and with different B-site cations.

Acknowledgments

I would like to thank my research advisor, Dr. Patrick Woodward, for the opportunity to conduct research in his laboratory. I am truly grateful for all of his insightful help and feedback. His guidance and the time I have spent with his research group have been major influences in my decision to pursue graduate study.

I would like to thank Dr. Jie Xiong for helping with the start of this project and training me on many of the lab techniques necessary to succeed. I would also like to thank Phuong Tran for her help with collection and interpretation of magnetic data, as well as being my "go to" whenever I have a question. Additionally, I would like to thank the entire Woodward research group: Dr. Andrew Sharitz, Eric McClure, Matt Gray, David Merz, and Jackson Majher for their mentorship, advice, and laboratory instruction.

I thank Dr. Cowan for being a part of my thesis review committee. His inorganic chemistry classes have been major determining factors for my desire to focus my graduate studies towards inorganic chemistry.

I would like to thank Dr. Katie Moga and the entirety of the General Chemistry Lab Supervisor team for their mentorship throughout my time teaching. Their guidance has also been a major factor in my decision to continue my studies by going to graduate school.

Finally, I would like to thank my family and friends, especially my parents and grandparents. Their continuous and unconditional support has made my undergraduate education possible, and their excitement for my research is what has helped me to stay motivated throughout this entire project.

1. Introduction

Double perovskites have the general formula $A_2BB'O_6$ and are characterized by a network of corner connected octahedral with the A-site cation situated in the cavities formed within the octahedral framework. The ideal double perovskite structure consists of a rock-salt ordering pattern of the B and B′ cations, however disorder occurs on occasion. Figure 1 shows the simplest form of a cubic double perovskite. There are other variations of this structure that will also be discussed such as: tetragonal, monoclinic, and trigonal double perovskites. Examples of these can be seen in Figures 2, 3, and 4. A major difference between the cubic, tetragonal, and monoclinic is the pattern of octahedral tilting, which lowers the symmetry in various ways depending on the combination of in-phase and/or out-of-phase tilting. These structures provide a great platform to study the magnetic interactions among 5*d* transition metal ions because the structure can accommodate many elements from the periodic table.

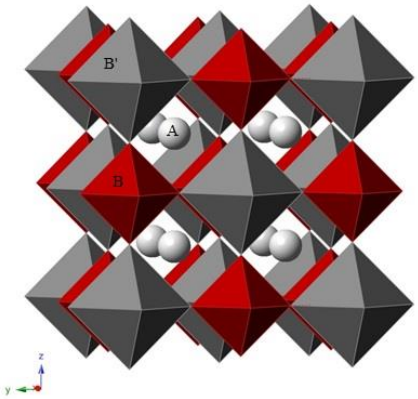

Figure 1: Cubic Double Perovskite

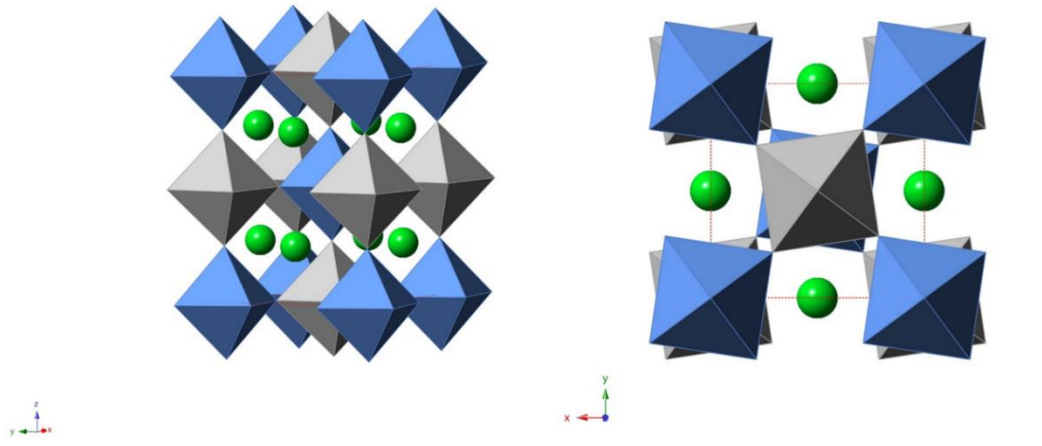

Figure 2: Tetragonal double perovskite structure, with octahedral tilt system $a^0a^0c^-$, shown looking down the a and c axes

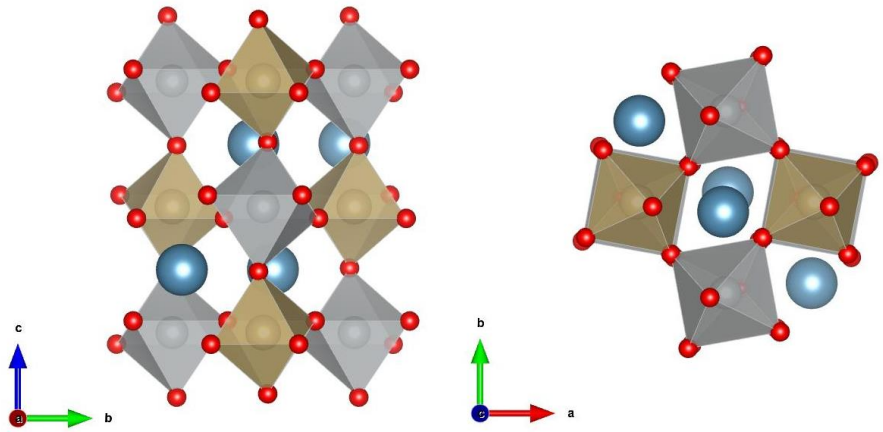

Figure 3: Monoclinic double perovskite structure, with octahedral tilt system $a^-a^-c^+$, shown looking down the a and c unit cell axes

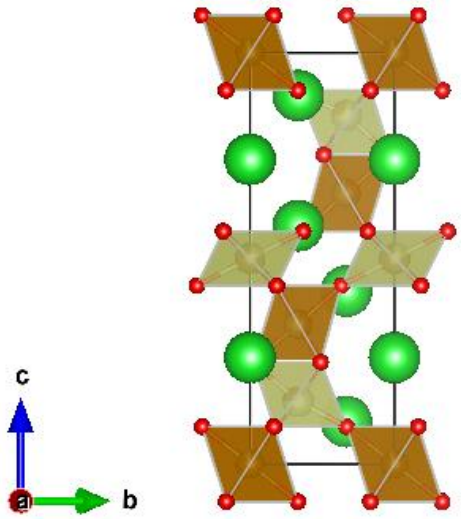

Figure 4: Trigonal structure with space group symmetry P-3m1, shown looking down the a *axis.*

The geometric stability of these structures can often be classified by a value known as the Goldschmidt Tolerance Factor, t, defined below:

$$t = \frac{r_A + r_O}{\sqrt{2} \times (\frac{r_B + r_{B\prime}}{2} + r_O)}$$

where r_A, r_B, $r_{B'}$, r_O are the radii of the *A*, *B* and *B'* cations, and oxygen ion, respectively; *t*=1 for the cubic double perovskite. When *t* falls below 1, octahedral tilting tends to set in due to the *A*-site cation being too small. This can at first lead to a tetragonal structure and then with increased octahedral tilting, the monoclinic structure. When *t* is greater than 1, the corner connectivity of the octahedra framework in the double perovskite has to break to some extent to accommodate the large *A*-site cation. This results in hexagonal or trigonal perovskite structures featuring dimers or trimers of face-sharing octahedra connected by sharing of common corners.

Transition metal oxides containing 5*d* ions are of particular interest because they have been observed to have diverse magnetic properties. These unique magnetic characteristics of 5*d* transition metal oxides are thought to be dependent on the strong spin-orbit coupling and the large spatial extent of the *d*-orbitals.

The typical approach to studying magnetism is through the use of susceptibility measurements when varying temperatures. By studying the paramagnetic region of these measurements, more information about the magnetic behavior can be determined through the use of the Curie-Weiss law:

$$\chi = \frac{C}{T - \theta}$$

where χ is the magnetic susceptibility, C is a material specific Curie constant, T is the temperature, and ϴ is the Weiss constant, which is a measure of the strength of the coupling between magnetic ions. A negative Weiss constant indicates antiferromagnetic coupling, while a positive Weiss constant indicates ferromagnetic coupling. The Curie constant, C, can be related to the effective moment, $\mu_{eff,}$ by the equation:

$$\mu_{eff} = 2.84\sqrt{C}$$

For $5d^1$ and $5d^2$ electron configurations, magnetic properties have been found such as ferromagnetism, antiferromagnetism, and spin glass.[4] In d^1 electron configurations, there is only one unpaired electron in the d-orbitals. The magnetism of these compounds is largely due to the structure of the compound and magnetic interactions that can occur with surrounding atoms. The Re^{6+} cation has a d^1 electron configuration and will be explored.

5*d* transition metals with the d^4 electron configuration, such as Ir^{5+}, also have been known to display interesting magnetic characteristics. When Ir^{5+} is in a cubic field, it is expected to have a low-spin $t_{2g}^4 e_g^0$ (S = 1) electron configuration. However, strong spin-orbit coupling will split the t_{2g} orbitals into energetically favorable four $J_{eff} = 3/2$ and two $J_{eff} = 1/2$ states. The band that is lowest in energy will be filled with the d^4 electrons, resulting in an electrically insulating $J_{eff} = 0$ singlet ground state. This can be seen in Figure 5.[5] By synthesizing compounds containing the Ir^{5+} ion, the magnetism of these compounds can be explored.

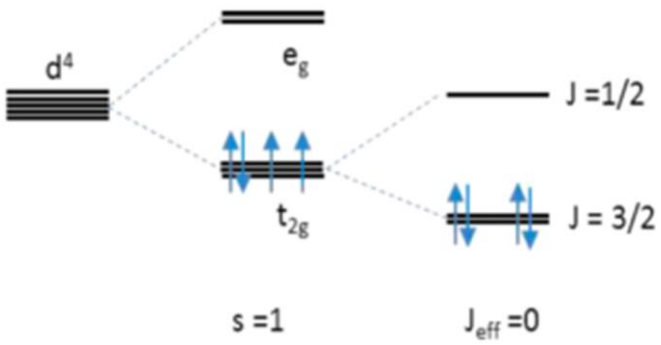

Figure 5: Splitting of the t_{2g} orbitals as seen in Ir^{5+}

2. Experimental

2.1 Synthesis

Stoichiometric amounts of the solid reagents were combined under ambient conditions for each of the compounds made, with the exception of Sr_2ZnReO_6, which was combined in an

argon filled glove box. Lanthanum oxide and magnesium oxide were heated to 1000 ^{o}C for 10 hours in air prior to synthesis to ensure reagent purity. Reagents were ground with a mortar and pestle for approximately 20 minutes. They were then heated in alumina crucibles to various temperatures ranging from 900 ^{o}C to 1300 ^{o}C in ~24 hour increments. The Sr_2ZnReO_6 was heated in an evacuated quartz tube. The products were checked for purity using XRPD between each heating.

2.2 Materials

Table 1: Reagents used in solid state synthesis

Reagents	Supplier	Purity
$BaCO_3$	Alfa Aesar	99.99%
BaO	Sigma Aldrich	99.99%
BaO_2	Mallinckrodt	99%
Ir	Alfa Aesar	99.9%
IrO_2	Alfa Aesar	99.99%
La_2O_3	GFS Chemical, Inc.	99.99%
Lu_2O_3	Alfa Aesar	99%
MgO	Allied Chemical	99.9%
Nb_2O_5	Alfa Aesar	99.5%
NiO	Johnson Matthey	99%
ReO_3	Alfa Aesar	99.9%
$SrCO_3$	Sigma Aldrich	99.9%
SrO	Sigma Aldrich	99.9%
Ta_2O_5	Strem Chemicals	99.8%
ZnO	Alfa Aesar	99.99%

2.2.1 Ba_2LuIrO_6

Synthesis of Ba_2LuIrO_6 was carried out according to the following equation:

$$4\ BaCO_3\,(s) + Lu_2O_3\,(s) + 2\ Ir\ (s) + 5/2\ O_2\ (g) \rightarrow 2\ Ba_2LuIrO_6\,(s) + 4\ CO_2(g)$$

Reactants were ground with a mortar and pestle for 20 minutes under ambient conditions. The powder was heated successively starting at 800 ^{o}C for 24 hours, 850 ^{o}C for 24 hours, 1200 ^{o}C for 48 hours, and finally 1250 ^{o}C for 24 hours.

2.2.2 $SrLaZnIrO_6$

Synthesis of $SrLaZnIrO_6$ was carried out according to the following equation:

$$La_2O_3\,(s) + 2\,SrCO_3\,(s) + 2\,ZnO\,(s) + 2\,Ir\,(s) + 5/2\,O_2\,(g) \rightarrow 2\,SrLaZnIrO_6\,(s) + 2\,CO_2\,(g)$$

Reactants were ground with a mortar and pestle for 20 minutes under ambient conditions. The powder was heated at 1000 ^oC for 12 hours and 1100 ^oC for 12 hours.

2.2.3 $SrLaMgIrO_6$

Synthesis of $SrLaMgIrO_6$ was carried out according to the following equation:

$$La_2O_3\,(s) + 2\,SrCO_3(s) + 2\,MgO\,(s) + 2\,Ir\,(s) + 5/2\,O_2\,(g) \rightarrow 2\,SrLaMgIrO_6\,(s) + 2\,CO_2\,(g)$$

Reactants were ground with a mortar and pestle for 20 minutes under ambient conditions. The powder was heated at 1000 ^oC, 1100 ^oC, and 1200 ^oC each in 24 hour increments.

2.2.4 $SrLaNiIrO_6$

Synthesis of $SrLaNiIrO_6$ was carried out according to the following equation:

$$La_2O_3\,(s) + 2\,SrCO_3\,(s) + 2\,NiO\,(s) + 2\,IrO_2\,(s) + 1/2\,O_2\,(g) \rightarrow 2\,SrLaNiIrO_6\,(s) + 2\,CO_2\,(g)$$

Reactants were ground with a mortar and pestle for 20 minutes under ambient conditions. The powder was heated at 900 ^oC, 1000 ^oC, and 1100 ^oC each in 24 hour increments.

2.2.5 $SrLaNiNbO_6$

Synthesis of $SrLaNiNbO_6$ was carried out according to the following equation:

$$La_2O_3\,(s) + 2\,SrCO_3\,(s) + 2\,NiO\,(s) + Nb_2O_5\,(s) \rightarrow 2\,SrLaNiNbO_6\,(s) + 2\,CO_2\,(g)$$

Reactants were ground with a mortar and pestle for 20 minutes under ambient conditions. The powder was heated at 900 ^oC for 12 hours, 1000 ^oC for 24 hours, and 1200 ^oC for 24 hours.

2.2.6 $SrLaNiTaO_6$

Synthesis of $SrLaNiTaO_6$ was carried out according to the following equation:

$$La_2O_3\,(s) + 2\,SrCO_3\,(s) + 2\,NiO\,(s) + Ta_2O_5\,(s) \rightarrow 2\,SrLaNiTaO_6\,(s) + 2\,CO_2\,(g)$$

Reactants were ground with a mortar and pestle for 20 minutes under ambient conditions. The powder was heated at 900 ^{o}C for 12 hours, 1000 ^{o}C for 24 hours, 1100 ^{o}C for 24 hours, and 1200 ^{o}C for 24 hours.

2.2.7 Ba_2FeIrO_6

Synthesis of Ba_2FeIrO_6 was carried out according to the following equation:

$$4\ BaCO_3\ (s) + Fe_2O_3\ (s) + 2\ IrO_2\ (s) + 1/2\ O_2\ (g) \rightarrow 2\ Ba_2FeIrO_6\ (s) + 4\ CO_2\ (g)$$

Reactants were ground with a mortar and pestle for 20 minutes under ambient conditions. The powder was heated successively at 900 ^{o}C for 24 hours, 1000 ^{o}C for 24 hours, and 1100 ^{o}C for 48 hours. This synthesis was also carried out in an argon filled glove box and heated in an evacuated quartz tube using barium oxide and barium peroxide. This synthesis yielded similar product purity and the chemical equation can be seen below.

$$3\ BaO\ (s) + BaO_2\ (s) + Fe_2O_3\ (s) + 2\ IrO_2\ (s) \rightarrow 2\ Ba_2FeIrO_6\ (s)$$

2.2.8 $Ba_3Fe_2IrO_9$

Synthesis of $Ba_3Fe_2IrO_9$ was carried out according to the following equation:

$$3\ BaCO_3\ (s) + Fe_2O_3\ (s) + IrO_2\ (s)\ + 1/2\ O_2\ (g)\ \rightarrow Ba_3Fe_2IrO_9\ (s) +\ 3\ CO_2\ (g)$$

Reactants were ground with a mortar and pestle for 20 minutes under ambient conditions. The powder was heated successively at 900 ^{o}C for 24 hours, and 1100 ^{o}C for 24 hours. This synthesis was also carried out in an argon filled glove box and heated in an evacuated quartz tube using barium oxide and barium peroxide. This synthesis yielded similar product purity and the chemical equation can be seen below.

$$2\ BaO\ (s) + BaO_2\ (s)\ + Fe_2O_3\ (s) + IrO_2\ (s)\ \rightarrow Ba_3Fe_2IrO_9\ (s)$$

2.2.9 Sr_2ZnReO_6

Synthesis of Sr_2ZnReO_6 was carried out according to the following equation:

$$2\ SrO\ (s) + ZnO\ (s) + ReO_3\ (s) \rightarrow Sr_2ZnReO_6\ (s)$$

Reactants were ground with a mortar and pestle for 20 minutes in an argon glove box. The powder was heated in an evacuated quartz tube at 900 ^{o}C for 24 hours and again heated in an evacuated quartz tube at 950 ^{o}C for 12 hours.

2.3 Crystal Structure Determination

All samples were checked for purity between each heating using a Rigaku Miniflex II benchtop X-ray powder diffractometer. After successive heatings and Miniflex XRPD measurements concluded that samples were completely reacted, XRPD data was then collected on a Bruker D8 X-ray powder diffractometer in Johannsson mode using a Kα1 monochromator. The Sr_2ZnReO_6 was measured using a Bruker D8 X-ray powder diffractometer in Bragg-Brentano mode.

Crystal structure determination was carried out by doing XRPD data refinements using TOPAS-6 Academic. First, Pawley refinements were done to determine the correct unit cell parameters, and these were then used in carrying out Rietveld refinements to determine atomic positions and occupancies. Jade was often used in combination with TOPAS-6 Academic in order to more quickly and estimate unit cell parameters for impurities. CMPR was also used in order to index XRPD data when difficulties arose in determining unit cell parameters. CrystalMaker and VESTA were used in generating images of these refined structures.

2.4 Magnetic Properties Determination

Samples were then analyzed using a Superconducting Quantum Interference Device (SQUID). Magnetic Susceptibility was measured between temperatures of 2 K to 400 K in zero-

field cooled and field cooled mode with a field of 1000 Oested (Oe) for each of the compounds except Sr_2ZnReO_6, which was measured with 10 kOe.

3. Results and Discussion

3.1 Ba_2LuIrO_6

Ba_2LuIrO_6 has been previously synthesized by other groups and has been reported as monoclinic, with the space group $P2_1/n$ with a = 5.8689 Å, b = 5.8608 Å, and c = 8.285 Å.[6] However, the calculated tolerance factor is 1.013, which makes this monoclinic space group assignment unlikely. A literature report on the space group of Ba_2MIrO_6 (M = La, Y) casts doubt on their monoclinic assignments, citing that the Ba^{2+} ion is too large and therefore the space group will have a higher symmetry.[7] It is likely that this is the case with the Ba_2LuIrO_6 as well. The synthesis methods resulted in a relatively pure compound, with the only impurity being Lu_2O_3 in 3.55 +/− 0.09% by mass. The XRPD pattern for this compound can be seen in Figure 6. It was fit to a cubic Fm-3m space group with a = 8.2960(9) Å. Atomic positions and bond lengths are summarized in Table 2.

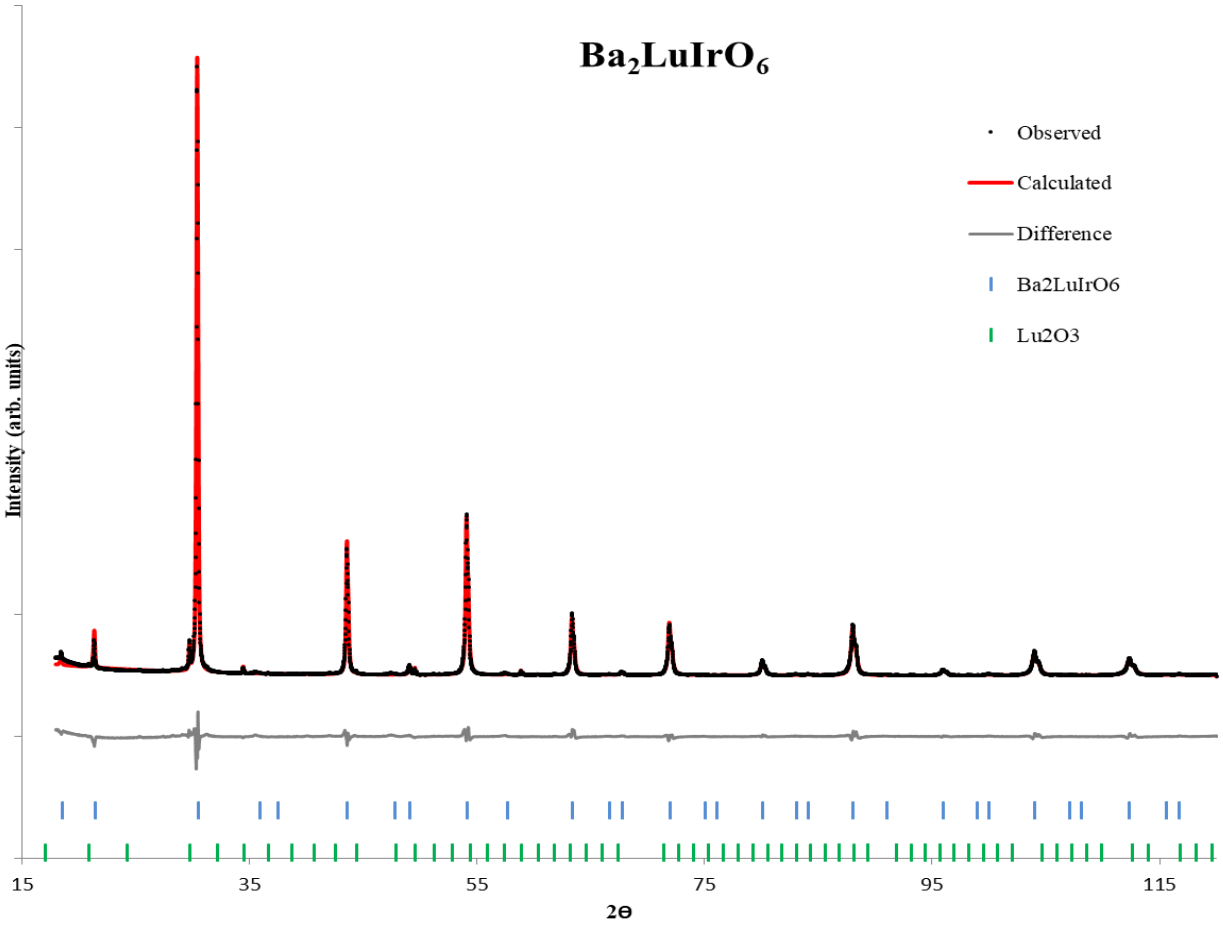

Figure 6: X-ray Diffraction data for Ba_2LuIrO_6 fit with slight Lu_2O_3 impurity

Table 2: Structural Refinement Data for Ba_2LuIrO_6

	Ba_2LuIrO_6
Space group	Fm-3m
a (Å)	8.2960(9)
V (Å^3)	570.97(1)
R_{wp}	12.042
Ba	(¼, ¼, ¼)
Beq	0.0040
Lu	(0, 0, 0)
Lu occ	0.997(4)
Ir occ	0.003(4)
Beq	0.0412
Ir	(1/2 , 0, 0)
Ir occ	0.997(4)
Lu occ	0.003(4)
Beq	0.0412
O1	(0.2762(9), 0,0)

Beq	0.0146
Bond lengths	
Ba-O	2.9412(7) Å
Lu-O	2.291(8) Å
Ir-O	1.857(8) Å

It is also important to note that Ba_2ScIrO_6 was also originally reported as monoclinic; this was recently corrected by a different article stating that it is actually cubic *Fm*-3*m* as well.[5] Magnetic measurements for Ba_2LuIrO_6 can be seen in Figures 7 and 8.

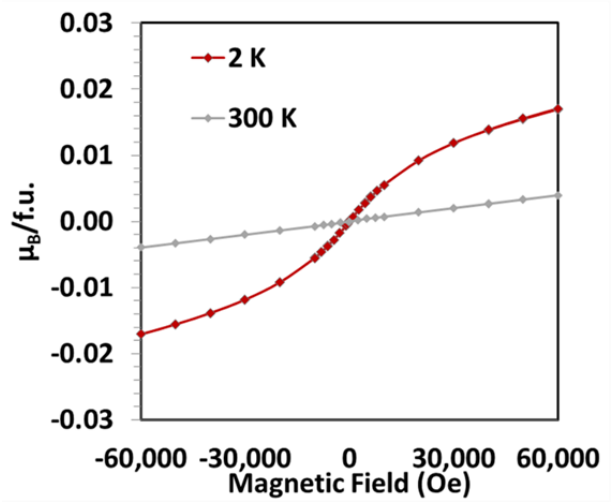

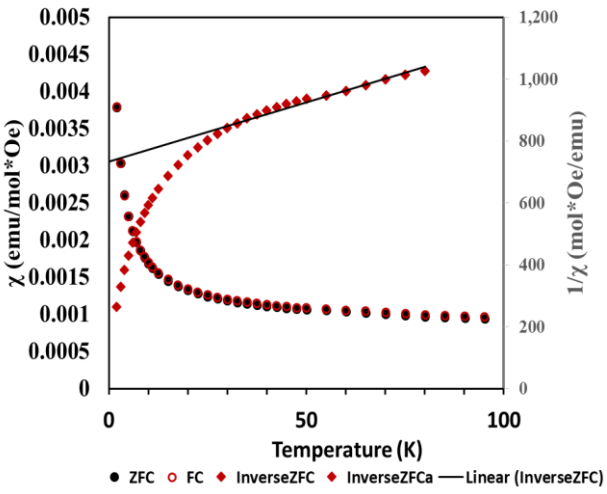

Figure 7: Magnetization (M) of Ba_2LuIrO_6 measured when a magnetic field (H) is applied

Figure 8: Magnetic Susceptibility Measurements for Ba_2LuIrO_6

No long range magnetic order was observed in the magnetic susceptibility data. In addition, the magnetic susceptibility does not follow the linear Curie-Weiss behavior. The lack of magnetic transition and non-linear Curie-Weis behavior appear to be a signature of Ir^{5+}, also observed in a previous work on cubic Ba_2ScIrO_6. Ba_2ScIrO_6 had a Weiss constant of approximately 0 K and an effective moment of 0.39 μ_B.[5] These values were obtained by using a

non-linear fit to the data with corrections for the diamagnetic contributions, d, and the temperature-independent contributions, TIP. Using the non-linear fit equation:

$$\chi = \left[(1-d) \times \frac{C}{T-\theta} + TIP\right] + d \times \left(\frac{0.375}{T}\right)$$

the magnetic susceptibility data was able to be fit relatively well with an R^2 value of 0.99. This fit, using a diamagnetic correction, of -0.05152 and a temperature-independent contribution of 2.16055×10^{-4}, yielded a ϴ value of approximately 0 K and an effective moment of 0.393 μ_B.

3.2 Monoclinic phases: $SrLaZnIrO_6$ and $SrLaMgIrO_6$

3.2.1 $SrLaZnIrO_6$

$SrLaZnIrO_6$ has been successfully synthesized using traditional solid-state techniques with successive heatings for 24 hours starting at 800 ^oC and increasing 100 ^oC for each heating, with a final maximum temperature of 1300 ^oC. XRPD data can be seen below in Figure 9. It has been fit to a monoclinic $P2_1/n$ space group (a = 5.623(8) Å, b = 5.6093(1) Å, c = 7.9322(2) Å, β = 90.024(8)). This space group experiences an out of phase tilt along the a and b axes, and an in-phase tilt along the c axis ($a^-a^-c^+$). The A-sites for this compound, as well as the other compounds containing La^{3+} and Sr^{2+} discussed, are made to be completely disordered in the Rietveld refinement due to the similar size of the La^{3+} and the Sr^{2+} cations and a charge difference of < 2. However, B-site cations are almost completely ordered because of the large difference in radii and charge between the Zn^{2+} and Ir^{5+} cations. Magnetic data was collected on the SQUID and can be seen below in Figure 10. This was fit using the Curie-Weiss Law and was found to be paramagnetic with an effective moment of 1.2151 μ_B and a Weiss constant of -

93.499 K, however it only followed the linear behavior of the Curie-Weiss Law up until 100 K, so the fit may be unreliable.

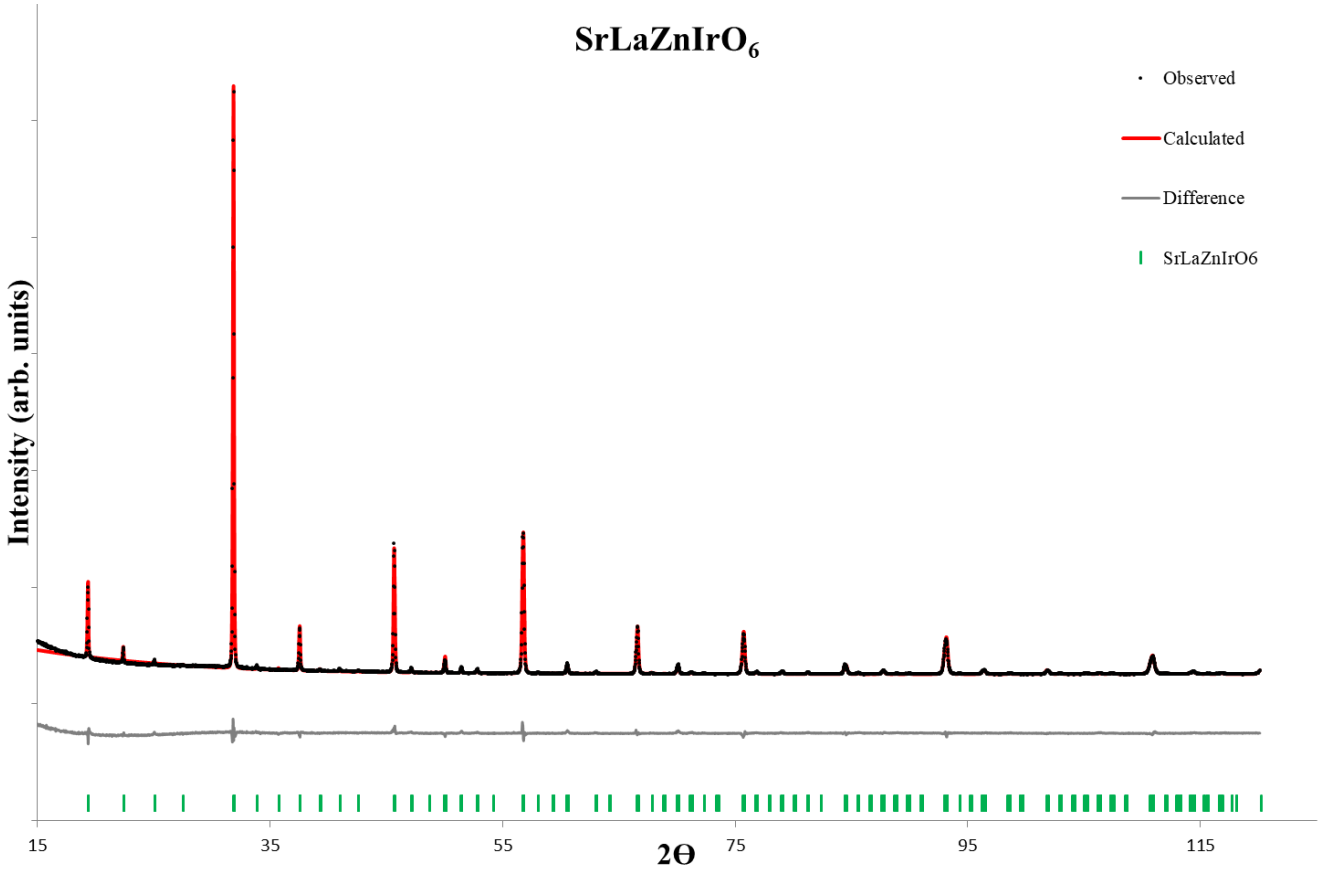

Figure 9: X-ray Diffraction data for $SrLaZnIrO_6$ fit to monoclinic $P2_1/n$ space group

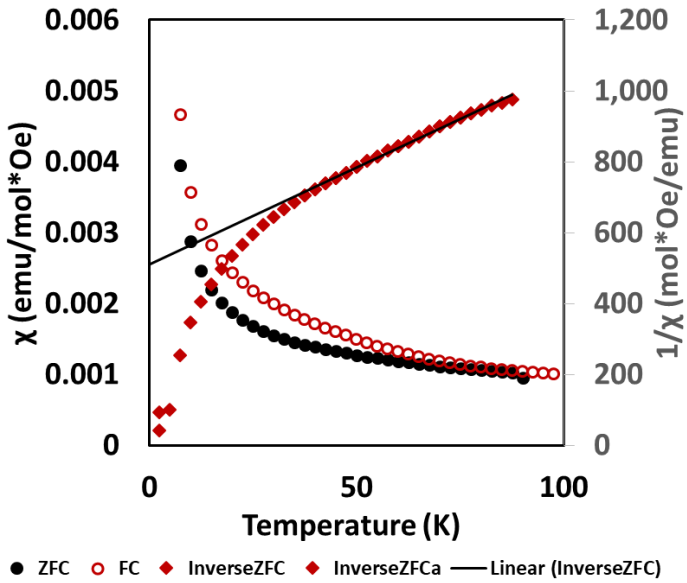

Figure 10: Magnetic Susceptibility measurements for $SrLaZnIrO_6$. No magnetic transitions were observed.

3.2.2 $SrLaMgIrO_6$

$SrLaMgIrO_6$ has been successfully synthesized using traditional solid-state techniques with successive heatings for 24 hours starting at 1000 ^oC and increasing 100 ^oC for each heating, with a final maximum temperature of 1200 ^oC. XRPD data can be seen in Figure 11. It has been fit to a monoclinic $P2_1/n$ space group (a = 5.5934(2) Å, b = 5.5893(2) Å, c = 7.9203(3) Å, β = 90.227(3). Again, the B-site cations are completely ordered because of the large differences between the Mg^{2+} and Ir^{5+} cations. Magnetic data was collected on the SQUID and can be seen below in Figure 12. No magnetic transition was observed. This was fit using the Curie-Weiss Law and was found to be paramagnetic with an effective moment of 1.4979 μ_B and a Weiss constant of -140.90 K, however it only followed the linear behavior of the Curie-Weiss Law up until 100 K, so the fit may be unreliable. It has been previously synthesized by other groups under high oxygen pressure and characterized with an orthorhombic unit cell with the parameters: a = 5.567 Å, b = 5.598 Å, c = 7.89 Å.[8]

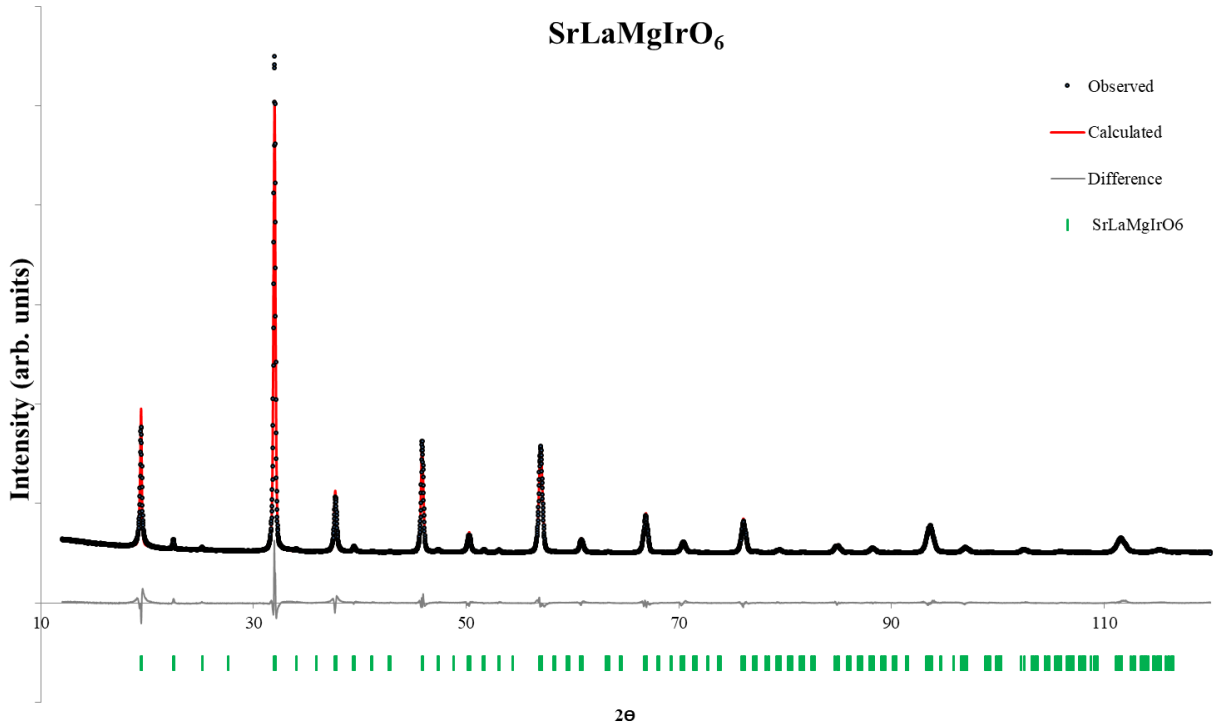

Figure 11: X-ray Diffraction data for $SrLaMgIrO_6$ fit to monoclinic $P2_1/n$ space group

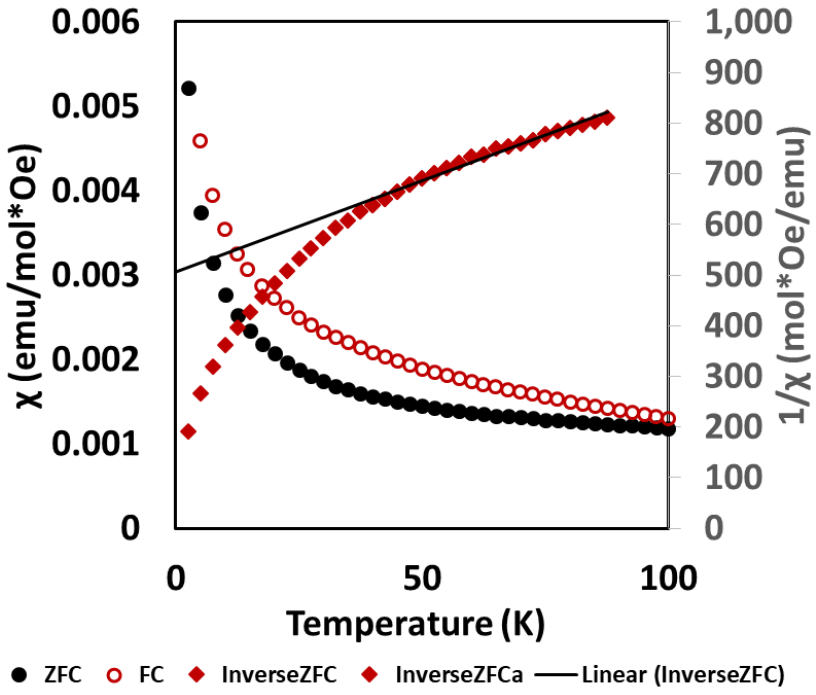

Figure 12: Magnetic Susceptibility measurements for $SrLaMgIrO_6$. No magnetic transitions were observed.

3.3 $SrLaNiIrO_6$, $SrLaNiNbO_6$, and $SrLaNiTaO_6$

$SrLaNiIrO_6$ has been successfully synthesized using traditional solid-state techniques with successive heatings for 24 hours starting at 900 ^oC and increasing 100 ^oC for each heating, with a final maximum temperature of 1100 ^oC. XRPD data can be seen below in Figure 13. It has been fit to a monoclinic $P2_1/n$ space group (a =5.5995(1) Å, b = 5.5747(2) Å, c = 7.8880(4) Å, β = 90.111(4)). As with the previous two compounds, the A-sites are completely disordered. The B-sites are almost entirely ordered due to the large difference in radii. Magnetic data was collected on the SQUID and can be seen below in Figures 14 and 15. A transition is seen at 50 K. This was fit using the Curie-Weiss Law and was found to be antiferromagnetic with an effective moment of 3.787 μ_B. However, the slight deviation between the zero-field cool and the field cool measurements hints at the possibility of spin glass behavior, so heat capacity measurements would be necessary in order to confirm this assignment. This is very similar to the structure of $SrLaCoIrO_6$. This was found to be $P2_1/n$ (a= 5.5988(1) Å , b = 5.5750(1) Å, c = 7.9029(2) Å, β = 89.989(6)) and was found to have an effective moment of μ_{eff} = 5.1(0).[9]

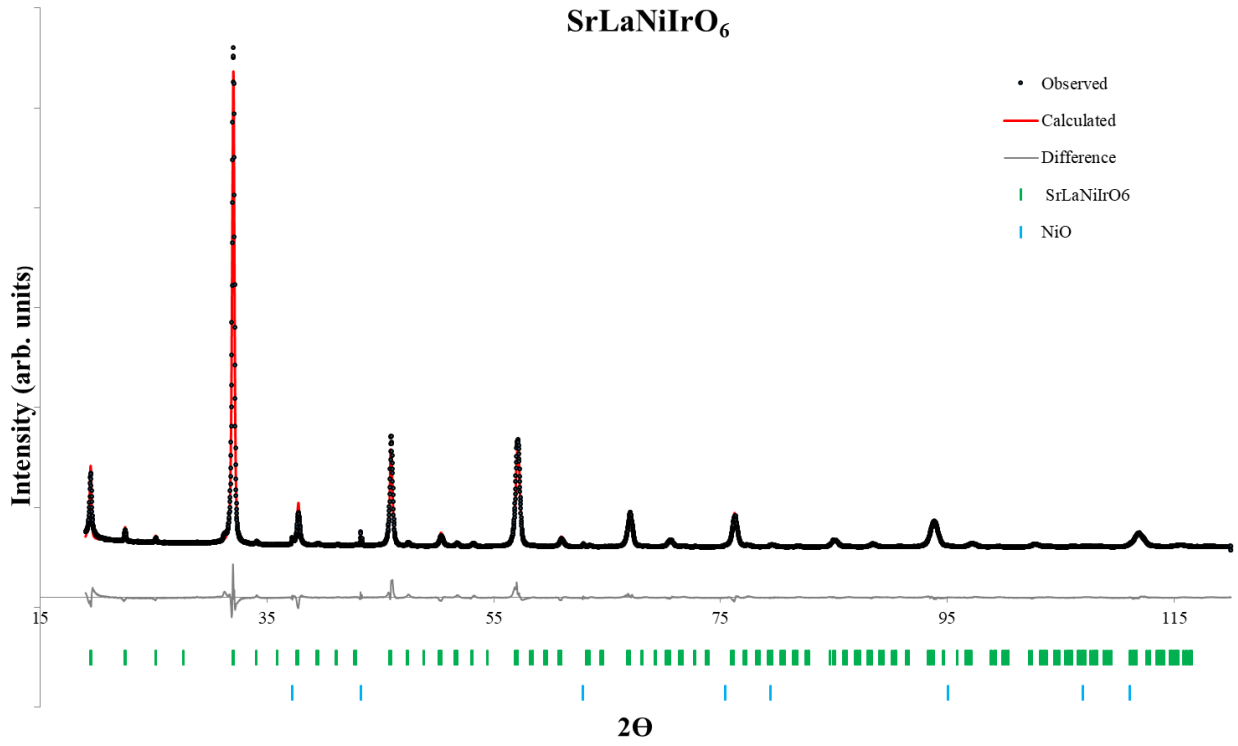

Figure 13: X-Ray Diffraction data for $SrLaNiIrO_6$ with slight NiO impurity.

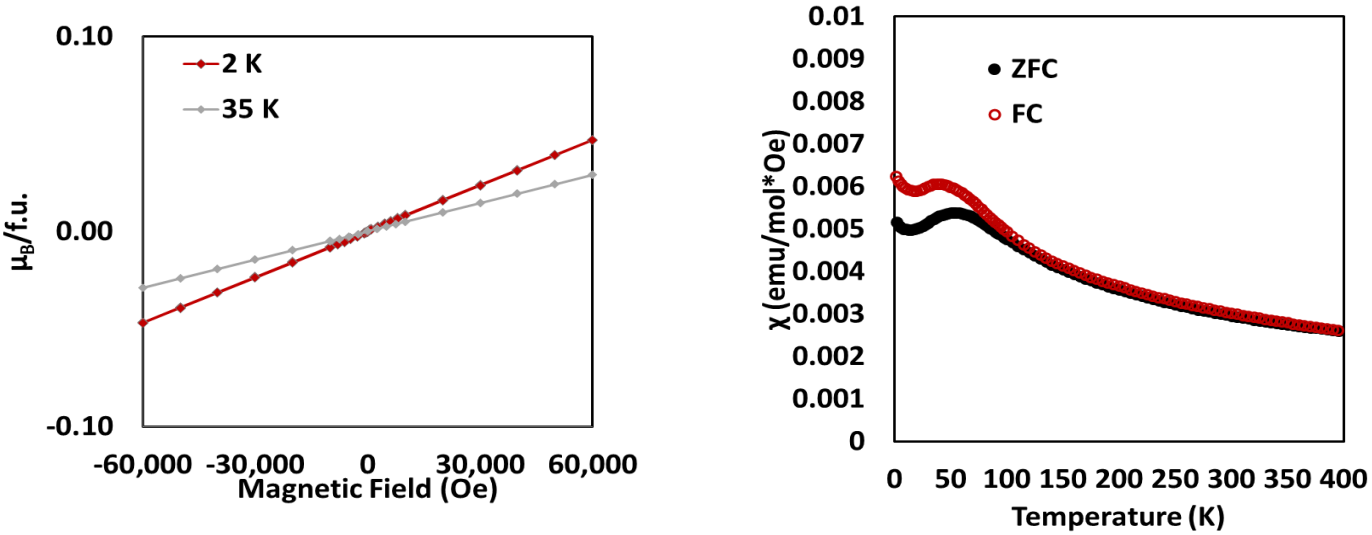

Figure 14: Magnetization (M) of $SrLaNiIrO_6$ measured when a magnetic field (H) is applied

Figure 15: Magnetic Susceptibility Measurements for $SrLaNiIrO_6$

In order to explore whether or not the antiferromagnetism seen in the $SrLaNiIrO_6$ was due to both the Ni^{2+} and Ir^{5+} ions interacting, or just the Ni^{2+} ions alone, two compounds,

$SrLaNiNbO_6$, and $SrLaNiTaO_6$, were synthesized as a point of comparison. Because Nb^{2+} and Ta^{2+} both have a d^0 electron configuration, it is expected that all magnetism seen in these compounds is due solely to the Ni^{2+} cation.

These compounds were synthesized using successive heatings starting at 900 ^oC with a maxiumum temperature of 1200 ^oC. They were each fit to the $P2_1/n$ space groups with lattice parameters of a = 5.6201(2) Å, b = 5.6218(2) Å, c = 7.9567(2) Å, β = 90.014(9) for the $SrLaNiNbO_6$ and a = 5.6271(1) Å, b = 5.6234(2) Å, c = 7.9655(1) Å, and β = 89.914(2) for the $SrLaNiTaO_6$. These can be seen in Figures 16 and 17 below. Magnetic measurements were taken on each of these compounds, which can be seen in Figures 18 and 19.

They each experience a transition around 50 K, similarly to the $SrLaNiIrO_6$. The effective moments were calculated to be 3.745 μ_B and 3.522 μ_B, respectively, using the Curie-Weiss Law. While these are slightly lower than what was observed in the $SrLaNiIrO_6$, they are still relatively similar and it is therefore possible that the magnetism seen in these compounds is a result of just the Ni^{2+} cation. However, it is important to note the vast difference in the Weiss constants. The Weiss constant is a measure of the strength of the coupling between magnetic ions. In the $SrLaNiNbO_6$ and $SrLaNiTaO_6$, the Ni^{2+} ions are the only magnetic ions and they are relatively far apart, which yields only a small amount of coupling, and values of -53.79 K and -46.00 K respectively. The $SrLaNiIrO_6$ had a more negative Weiss constant of -293.21 K, which indicates the presence of Ir^{5+} results in stronger antiferromagnetic coupling.

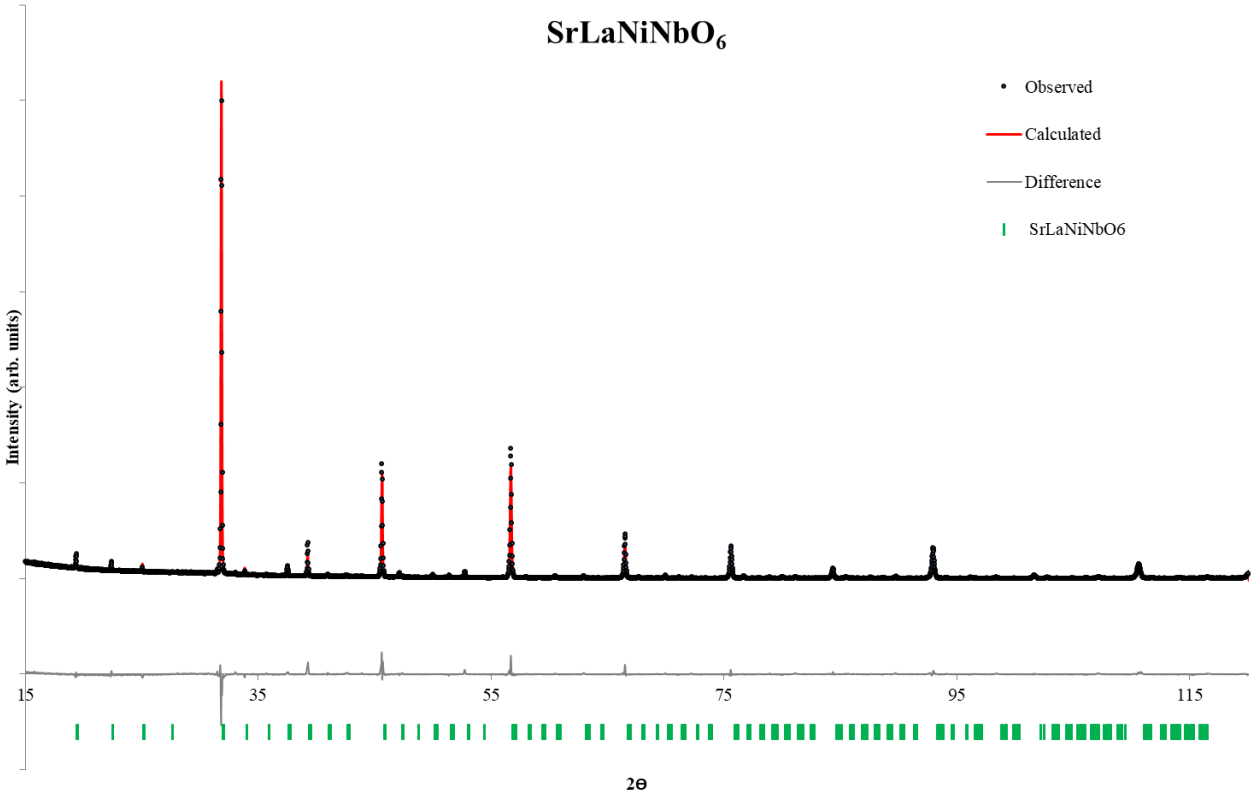

Figure 16: X-ray Diffraction data for $SrLaNiNbO_6$ fit to monoclinic $P2_1/n$ space group

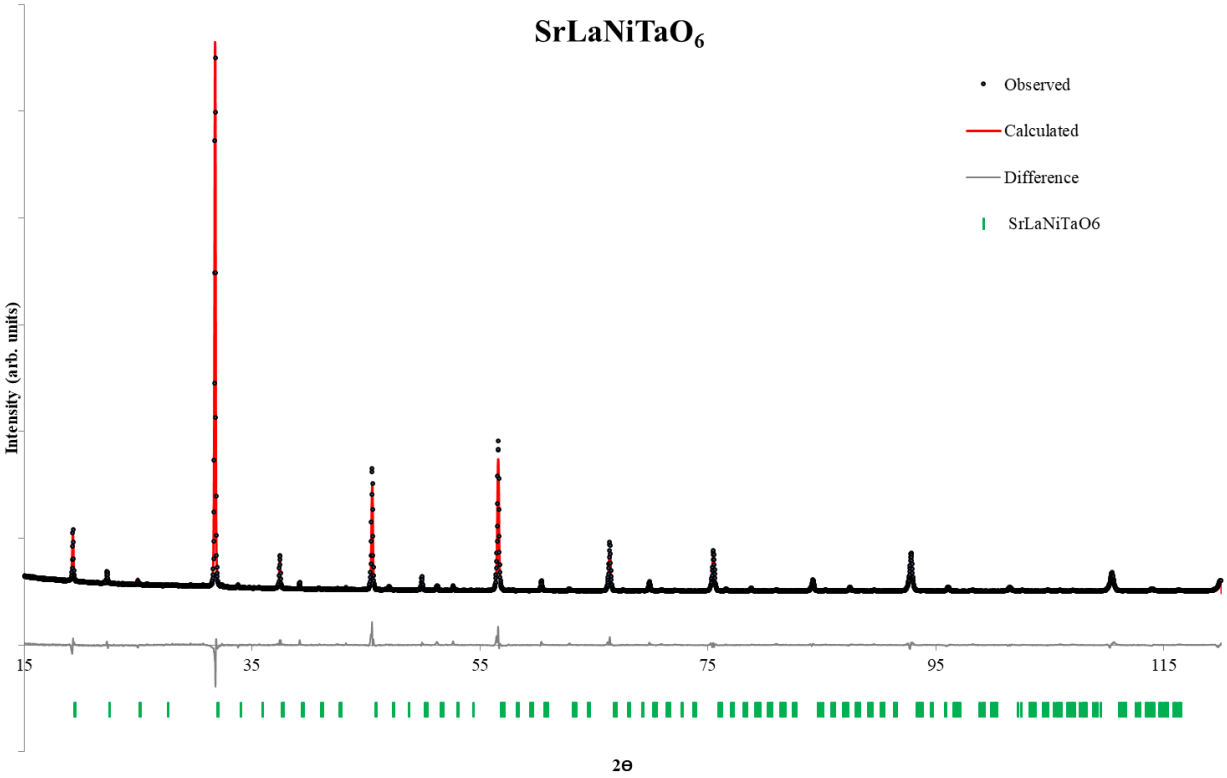

Figure 17: X-ray Diffraction data for $SrLaNiTaO_6$ fit to monoclinic $P2_1/n$ space group

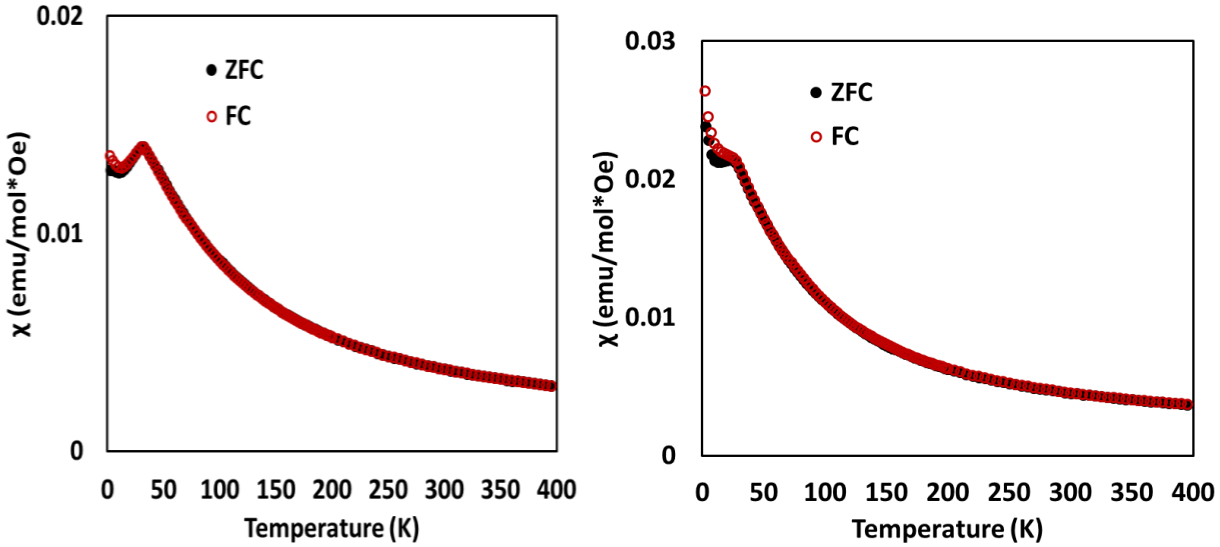

Figures 18 and 19: Magnetic Susceptibility measurements for $SrLaNiNbO_6$ and $SrLaNiTaO_6$.

3.4 Summarizing the monoclinic compounds synthesized

Shown below is a table summarizing the lattice parameters and atomic positions of each of the monoclinic compounds synthesized. In Table 4, the bond lengths and bond angles are compared. A disadvantage to using XRPD is that often the X-rays are not sensitive to lighter atoms, such as oxygen, in the presence of heavier atoms such as Ir^{5+}. Unfortunately this limits the reliability of these bond lengths and bond angles. However, they still offer some insight in comparing the compounds. Summarized in Table 5 are the effective moments and Weiss constants. Overall, it can be seen that the μ_{eff} values for all the compounds are very similar and therefore the contribution from the Ir^{5+} is negligible.

Table 3: Lattice parameters and bond lengths for monoclinic products

	$SrLaZnIrO_6$	$SrLaMgIrO_6$	$SrLaNiIrO_6$	$SrLaNiNbO_6$	$SrLaNiTaO_6$
Space group	$P2_1/n$				
a (Å)	5.623(8)	5.5934(2)	5.5747(2)	5.6201(2)	5.6271(1)
b (Å)	5.6093(1)	5.5893(2)	5.5995(1)	5.6218(2)	5.6234(2)
c (Å)	7.9322(2)	7.9203(3)	7.8880(4)	7.9567(2)	7.9655(1)
β	90.024(8)	90.227(3)	90.111(4)	90.014(9)	89.914(2)
V ($Å^3$)	250.12(1)	247.65(2)	246.23(1)	251.39(1)	252.05(1)
R_{wp}	8.796	13.972	10.877	7.730	10.065
A1	(0.002(1), 0.0259(2), 0.2544(7))	(-0.0120(7), 0.0201(2), 0.2330(3))	(0.006(1), 0.0119(5), 0.2527(8))	(0.005(5), -0.0175(5), 0.2407(3))	(0.0105(7), -0.0221(2), 0.2382(3))
La occ	0.59(1)	0.51(1)	0.51(1)	0.50(1)	0.50(1)
Sr occ	0.41(1)	0.49(1)	0.49(1)	0.50(1)	0.50(1)
Beq	0.4032	1*	0.1081	0.4441	0.05123
B1	(1/2, 0, 0)				
B occ	0.981(3)	0.866(2)	0.961(4)	0.80(1)	0.89(1)
B'occ	0.0190(3)	0.134(2)	0.039(4)	0.20(1)	0.11(1)
Beq	0.3709	1*	0.7782	0.5*	0.57526
B2	(1/2 , 0, 1/2)				
B occ	0.981(3)	0.866(2)	0.961(4)	0.80(1)	0.89(1)
B'occ	0.0190(3)	0.134(2)	0.039(4)	0.20(1)	0.11(1)
Beq	0.3709	1*	0.7782	0.5*	0.57526
O1	(0.228(4), 0.238(4), -0.012(5))	(0.247(9), 0.232(8), -0.15(6))	(0.227(3),0.202(3), 0.002(7))	(0.230(8), 0.253(9), 0.0027(8))	(0.270(6),0.245(3),-0.015(3))
Beq	1*	1*	1*	1*	1*
O2	(0.169(4), 0.182(4), 0.542(3))	(0.206(8), 0.224(9), 0.519(5))	(0.226(5), 0.233(4), 0.552(3))	(0.195(8), 0.157(6), 0.475(4))	(0.221(4),0.193(3), 0.486(3))
Beq	1*	1*	1.6541	1*	1*
O3	(0.434(4), -0.002(2), 0.227(2))	(0.451(8), 0.009(3), 0.396(4))	(0.51(1), 0.087(3), 0.220(2))	(0.549(5), -0.007(3),0.262(6))	(0.642(3), 0.008(2), 0.233(2))
Beq	1*	1*	1.5391	1*	1*

*Values have been fixed during refinement

Table 4: Bond lengths and Bond angles for monoclinic products

	$SrLaZnIrO_6$	$SrLaMgIrO_6$	$SrLaNiIrO_6$	$SrLaNiNbO_6$	$SrLaNiTaO_6$
A-O1	2.74(4)	2.60(5)	2.95(1)	3.00(7)	2.91(3)
A-O2	2.21(3)	2.70(5)	2.71(2)	2.37(4)	2.61(3)
A-O3	2.44(3)	2.53(3)	2.34(7)	2.59(4)	2.08(2)
M1-O1	2.03(3)	1.92(7)	1.19(4)	2.08(5)	1.89(3)
M1-O2	2.05(2)	2.05(9)	2.09(7)	2.22(5)	2.13(3)
M1-O3	1.84(2)	2.01(9)	2.07(2)	2.10(5)	2.03(3)
M2-O1	1.95(3)	2.02(3)	2.80(3)	1.90(5)	2.10(3)
M2-O2	2.15(3)	2.02(5)	1.86(5)	1.94(5)	1.91(3)
M2-O3	2.19(2)	2.03(5)	1.94(8)	1.91(5)	2.26(3)
M2-O1-M1	166.6(5)°	154.5(1)°	160.8(2)°	175(4)°	172.2(2)°
M1-O2-M2	139.5(5)°	152.0(4)°	171.2(3)°	146(3)°	159.6(1)°
M2-O3-M1	165.7(3)°	154.3(8)°	157.8(2)°	164.6(1)°	136.1(9)°

Table 5: Effective Moments and Weiss constants of monoclinic products

Compound	**Magnetic State**	**μ_{eff} (μ_b)**	**Θ (K)**	**Transition Temperature (K)**
$SrLaZnIrO_6$	Paramagnetic	1.215	-93.50	-
$SrLaMgIrO_6$	Paramagnetic	1.498	-140.90	-
$SrLaNiIrO_6$	Antiferromagnetic	3.787	-293.21	50 K
$SrLaNiNbO_6$	Antiferromagnetic	3.745	-53.79	50 K
$SrLaNiTaO_6$	Antiferromagnetic	3.522	-46.00	50 K

3.5 Trigonal Phases: $Ba_2Fe_{1.05}Ir_{0.95}O_6$ and $Ba_3Fe_{1.886}Ir_{1.114}O_9$

$Ba_2Fe_{1.05}Ir_{0.95}O_6$ and $Ba_3Fe_{1.886}Ir_{1.114}O_9$ were each synthesized using traditional solid-state techniques using stoichiometric amounts of reactants for Ba_2FeIrO_6 and $Ba_3Fe_2IrO_9$. XRPD

analysis was carried out on the Bruker D8 X-ray powder diffractometer in Johannsson mode and can be seen in Figures 20 and 21.

A Rietveld refinement was done on these compounds and they were found to be in the space group *P*-3*m*1, which is a trigonal structure. Hexagonal space groups, $P6_3/mmc$ and $P6_3mc$ were also tried; the trigonal space group *P*-3*m*1 yielded the best fit. $Ba_2Fe_{1.05}Ir_{0.95}O_6$ had lattice parameters of a = 5.74030(1) and c = 14.17439(8) and $Ba_3Fe_{1.886}Ir_{1.114}O_9$ had lattice parameters of a = 5.73488(1) and c = 14.1524(4). Table 6 illustrates the lattice parameters and atomic positions for these compounds. $Ba_2Fe_{1.257}Ir_{0.743}O_6$ had a slight impurity of Ba_2FeO_4, which is likely due to the fact that the targeted stoichiometry was $Ba_3Fe_2IrO_9$ and therefore there were excess reactants to form the impurity.

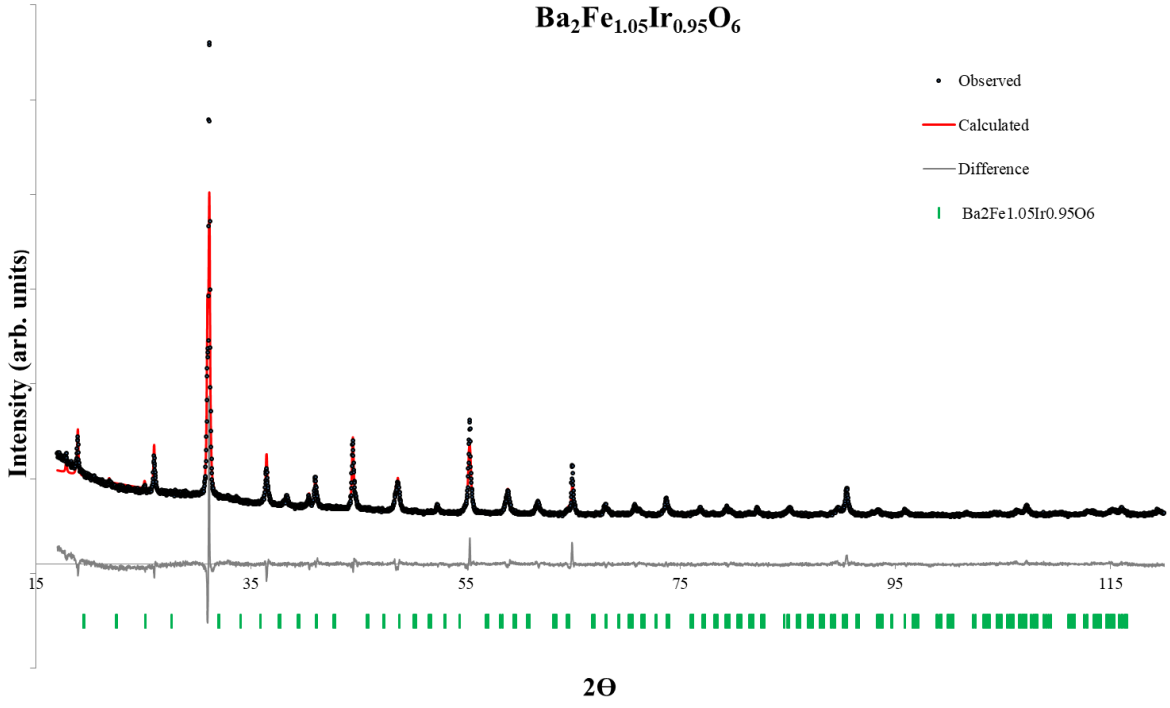

Figure 20: X-ray Diffraction Pattern for $Ba_2Fe_{1.05}Ir_{0.95}O_6$

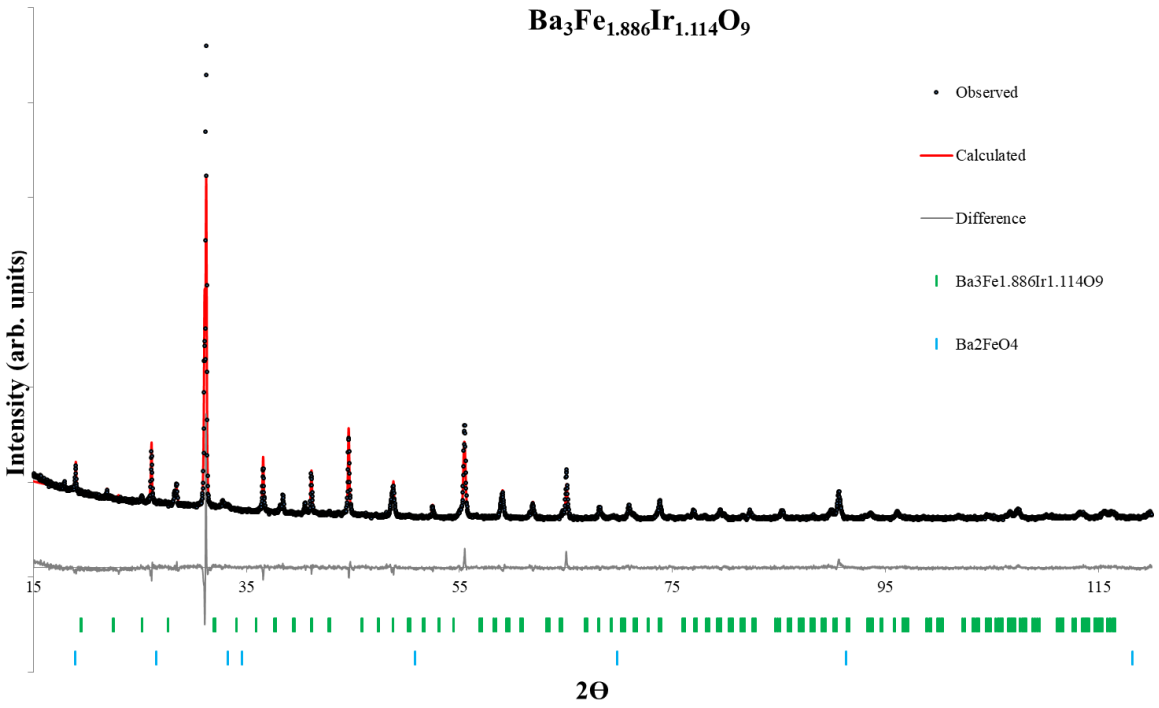

Figure 21: X-ray Diffraction pattern for $Ba_3Fe_{1.886}Ir_{1.114}O_9$

Table 6: Lattice Parameters and Atomic Positons for Trigonal Phases

	$Ba_2Fe_{1.05}Ir_{0.95}O_6$	$Ba_3Fe_{1.886}Ir_{1.114}O_9$
Space group	*P*-3*m*1	
a (Å)	5.74030(1)	5.73488(1)
c (Å)	14.17439(8)	14.1524(4)
V (Å^3)	404.47(3)	403.09(1)
R_{wp}	8.874	6.745
Ba 1	(0, 0, 0.2593(1))	(0, 0, 0.2609(8))
Ba 2	(1/3, 2/3, 0.1035(6))	(1/3, 2/3, 0.0919(8))
Ba 3	(1/3, 2/3, 0.4206(7))	(1/3, 2/3, 0.4134(8))
Fe 1	(0, 0, 0)	
Fe occ	0.90(4)	0.74(3)
Ir occ	0.10(4)	0.26(3)
Fe 2	(1/3, 2/3, 0.6597(8))	(1/3, 2/3, 0.662(6))
Fe occ	0.45(3)	0.51(2)
Ir occ	0.55(3)	0.49(1)
Ir 1	(0, 0, 1/2)	
Ir occ	0.21(4)	0.07(4)
Fe occ	0.79(4)	0.93(4)
Ir 2	(1/3, 2/3, 0.8478(7))	(1/3, 2/3, 0.8530(8))
Ir occ	0.73(3)	0.46(3)
Fe occ	0.27(3)	0.54(3)

O1	(0.51152, -0.51152, 0.247(5))	(0.51152, -0.51152, 0.252(4))
O2	(0.83453, -0.83453, 0.091(3))	(0.83453, -0.83453, 0.093(2))
O2	(0.81612, -0.81612, 0.433(3))	(0.81612, -0.81612, 0.435(2))

*B_{eq} values were fixed to 1 for refinements and oxygen positions in the x and y direction were fixed.

3.6 Sr_2ZnReO_6

Sr_2ZnReO_6 was successfully synthesized using traditional solid-state techniques prepared in an argon filled glove box. XRPD analysis was carried out on the Bruker D8 X-ray powder diffractometer in Bragg-Brentano mode, which can be seen in Figure 21. A Rietveld refinement was done on this compound and it was fit to a tetragonally distorted structure with *I*4/*m* symmetry ($a = b = 5.57667(3)$ Å, $c = 8.00314(7)$ Å). Sr_2ZnReO_6 is thought to be a mixed phase at room temperature, which is why a monoclinic phase is also observed in 3.3(1)%. The *I*4/*m* space group experiences an out of phase tilt ($a^0a^0c^+$), which can be seen down the *c*-axis. The B-site cations are almost entirely ordered, due to the large differences in their radii. This structure is very similar to the structure of Sr_2MgReO_6, which is expected due to the similar size of the Mg^{2+} and Zn^{2+} cations. It was also fit to the *I*4/*m* ($a = 5.5670$ Å, $c = 7.9318$ Å).[10]

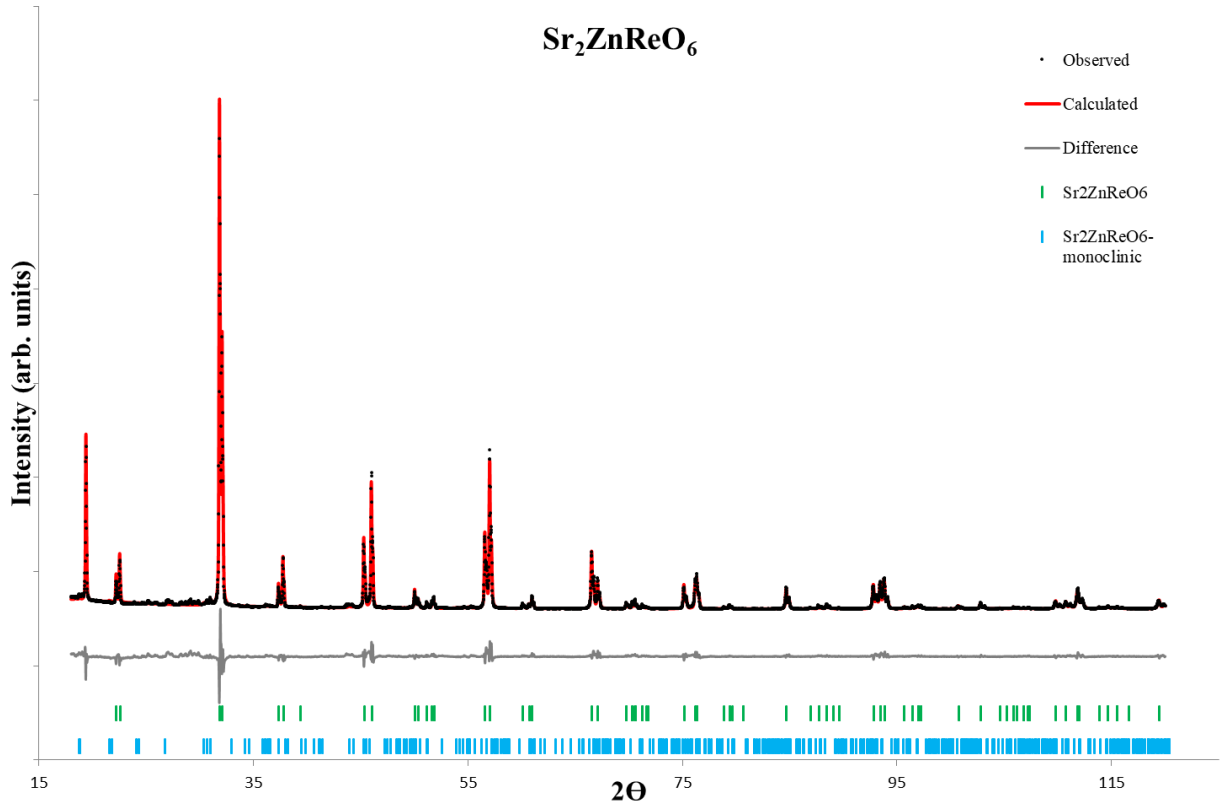

Figure 22:X-Ray Diffraction Scan of Sr_2ZnReO_6 fit to tetragonal I4/m space group

Table 7: Lattice parameters and atomic positions for Sr_2ZnReO_6

Sr_2ZnReO_6			
Space group	*I*4/*m*		
a (Å)	5.57667(3)	*c* (Å)	8.00314(7)
V (Å^3)	248.88(1)	B2	(0, 0, 0)
R_{wp}	11.852	B occ	0.985(2)
A1	(0, ½, ¼)	B'occ	0.015(2)
Beq	0.3	Beq	0.3
B1	(0, 0, ½)	O1	(0, 0.211(1), 0.287(1))
B occ	0.985(2)	Beq	1*
B'occ	0.015(2)	O2	(0, 0, 0.247(1))
Beq	0.3	Beq	1*

*Values were fixed during refinement

Table 8: Bond Lengths and Bond Angles for Sr_2ZnReO_6

	Sr_2ZnReO_6
Sr-O1 (Å)	2.606(2)
Sr-O2 (Å)	3.028(3)
Zn-O1 (Å)	2.022(8)
Zn-O2 (Å)	2.027(6)
Re-O1 (Å)	1.973(9)
Re-O2 (Å)	1.986(3)
Zn-O-Re	162.60(8)°

Magnetic data was collected on this compound, which can be seen in Figures 23 and 24.

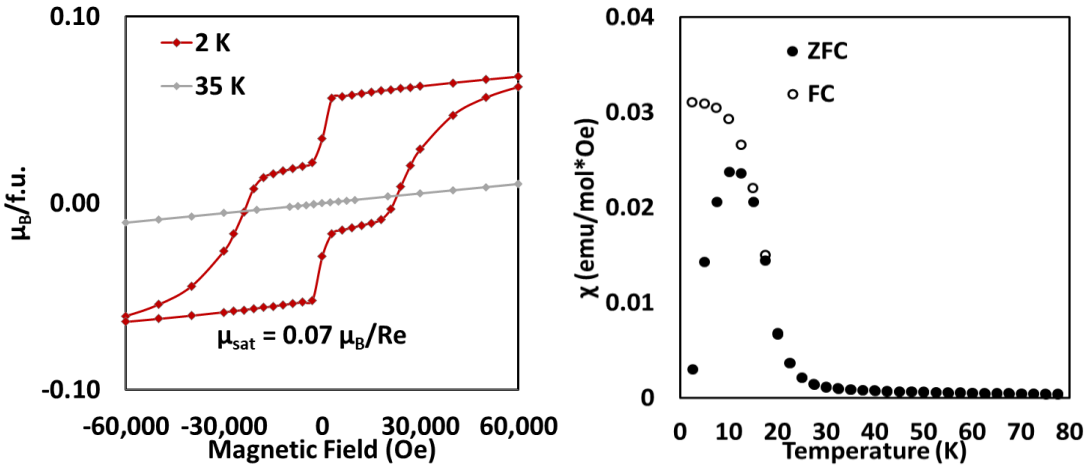

Figure 23: Magnetization (M) of Sr_2ZnReO_6 measured when a magnetic field (H) is applied

Figure 24: Magnetic Susceptibility Measurements for Sr_2ZnReO_6

Rhenium is in the d^1 electron configuration in this compound, as it is in the 6+ oxidation state. Due to the strong hysteresis loop seen in Figure 23 and the sharp rise in the magnetic susceptibility at 25 K in Figure 24, it can be concluded that this compound is ferromagnetic. The saturated moment obtained from the hysteresis is 0.07 μ_B, and the calculated effective moment from the magnetic susceptibility data is 0.5149 μ_B.. The Weiss constant, calculated from $1/\chi$ to be -2.097 K, seems inconsistent with the expected positive Weiss constant that indicates ferromagnetic behavior. However, it had been observed that several ferromagnetic rhenium d^1 compounds have negative Weiss constant.[11]

It is interesting to note how differently this compound behaves in comparison to Sr_2MgReO_6, which is a spin glass, despite having the same *d*-electron count and crystal structure.[10] Instead, it behaves more similarly to ferromagnetic Ba_2MReO_6 (M = Mg and Zn), which are both cubic structures. Ba_2MgReO_6 exhibits a transition at ~18 K, a saturated moment of 0.3 μ_B, and has an effective moment of 1.72(9) μ_B, and Ba_2ZnReO_6 exhibits a transition at 11 K and has a saturated moment of 0.1 μ_B.[11] The fact that the ferromagnetic ground state exists in both the cubic compound and the tetragonal Sr_2ZnReO_6 compound may suggest that this ground state is robust against structural change. However, it can be destabilized by going to a smaller unit cell of Sr_2MgReO_6.

4. Conclusion

Seven double perovskites, Ba_2LuIrO_6, $SrLaZnIrO_6$, $SrLaMgIrO_6$, $SrLaNiIrO_6$, $SrLaNiNbO_6$, $SrLaNiTaO_6$, and Sr_2ZnReO_6 and two trigonal structures, $Ba_2Fe_{1.05}Ir_{0.95}O_6$ and $Ba_2Fe_{1.257}Ir_{0.743}O_6$ were synthesized using traditional solid state techniques. Each of these is a novel material except for Ba_2LuIrO_6 and $SrLaMgIrO_6$, which had both been previously synthesized yet incorrectly characterized. Magnetic data had never been supplied on any these compounds. Characterization of these was carried out using X-ray powder diffraction, which helped to determine the crystals structures of each compound. Ba_2LuIrO_6 was determined to be cubic with the *Fm*-3*m* space group, Sr_2ZnReO_6 was determined to be tetragonal with the space group *I*4/*m*, $SrLaZnIrO_6$, $SrLaMgIrO_6$, $SrLaNiIrO_6$, $SrLaNiNbO_6$, and $SrLaNiTaO_6$ were found to be monoclinic with the space group $P2_1/n$, and $Ba_2Fe_{1.05}Ir_{0.95}O_6$ and $Ba_2Fe_{1.257}Ir_{0.743}O_6$ were found to be trigonal with the *P*-3*m*1 space group.

Each of the double perovskites were explored using SQUID magnetometry, in order to determine their magnetic characteristics. Ba_2LuIrO_6, $SrLaZnIrO_6$, and $SrLaMgIrO_6$ were each found to be paramagnetic with no long range magnetic order. $SrLaNiIrO_6$, $SrLaNiNbO_6$, and $SrLaNiTaO_6$ were each found to be antiferromagnetic with transitions occurring around 50 K. There is some speculation that $SrLaNiIrO_6$ may be spin glass, however, so heat capacity measurements would be necessary in order to confirm this assignment. Tetragonal Sr_2ZnReO_6 was determined to be ferromagnetic, which was observed in cubic Ba_2ZnReO_6, suggesting that this ferromagnetic ground state is robust against structural change.

Overall, this study gave insight in to the structural and magnetic characteristics of many novel materials. By further exploring these, as well as other 5d transition metal oxides, one may be able to more fully understand the governing characteristics that influence their exotic magnetic properties.

4. References

(1) Svoboda, C.; Randeria, M.; Trivedi, N. Orbital and Spin Order in Spin-Orbit Coupled D 1 and D 2 Double Perovskites. **2017**, 1–12.

(2) Ranjbar, B.; Reynolds, E.; Kayser, P.; Kennedy, B. J.; Hester, J. R.; Kimpton, J. A. Structural and Magnetic Properties of the Iridium Double Perovskites Ba 2 −X Sr X YIrO6. **2015**, *10476* (1).

(3) Svoboda, C.; Randeria, M.; Trivedi, N. Effective Magnetic Interactions in Spin-Orbit Coupled D 4 Mott Insulators. **2017**, *14409* (January).

(4) Tereshina, E. A.; Isnard, O.; Smekhova, A.; Andreev, A. V; Rogalev, A.; Khmelevskyi, S. Experimental and Theoretical Study of Magnetic Ordering and Local Atomic Polarization in Ru-Substituted Lu 2 Fe 17. **2014**, *94420*, 1–10.

(5) Kayser, P.; Kennedy, B. J.; Ranjbar, B.; Kimpton, J. A.; Synchrotron, A.; Road, B.; Avdeev, M. Spin − Orbit Coupling Controlled Ground State in the Ir (V) Perovskites A2ScIrO6 (A= Ba or Sr). **2017**, *6* (V), 6–11.

(6) Wakeshima, M.; Harada, D.; Hinatsu, Y. Crystal Structures and Magnetic Properties of Ordered Perovskites A R Ir O (A5Sr, Ba; R5Sc, Y, La, Lu). **1999**, *287*, 130–136.

(7) Fu, W. T.; Ijdo, D. J. W. Re-Examination of the Structure of Ba 2 MIrO 6 (M = La , Y): Space Group Revised. **2005**, *394*, 10–13.

(8) Walewski, M.; Buffat, B.; Demazeau, G.; Wagner, F.; Pouchard, M.; Hagenmuller, P. Preparation, Magnetic and Mossbauer Resonance Investigation of Some Perovskite-Type

Oxides Containing Iridium +V. *Mater. Res. Bull.* **1983**, *18* (7), 881–887.
(9) Narayanan, N.; Mikhailova, D.; Senyshyn, A.; Trots, D. M.; Laskowski, R.; Blaha, P.; Schwarz, K.; Fuess, H. Temperature and Composition Dependence of Crystal Structures and Magnetic and Electronic Properties of the Double Perovskites La 2 − X Sr X CoIrO 6 (0 ∋ X ∋ 2). **2010**, *6*, 1–12.
(10) Wiebe, C. R.; Greedan, J. E.; Kyriakou, P. P.; Luke, G. M.; Gardner, J. S.; Fukaya, A.; Russo, P. L.; Savici, A. T.; Uemura, Y. J. Frustration-Driven Spin Freezing in the S = 1/2 Fcc Perovskite Sr 2 MgReO 6. *Phys. Rev. B* **2003**, No. 68, 1–10.
(11) Marjerrison, C. A.; Thompson, C. M.; Sala, G.; Maharaj, D. D.; Kermarrec, E.; Cai, Y.; Hallas, A. M.; Wilson, M. N.; Munsie, T. J. S.; Granroth, G. E.; et al. Cubic Re6+ (5d1) Double Perovskites, Ba2MgReO6,Ba2ZnReO6, and Ba2Y2/3ReO6: Magnetism, Heat Capacity, μSR, and Neutron Scattering Studies and Comparison with Theory. *Inorg. Chem.* **2016**, No. 55, 10701–10713.